Evolution of dark state of an open atomic system in constant intensity laser field

A. J. Krmpot,* M. Radonjić, S. M. Ćuk, S. N. Nikolić, Z. D. Grujić, and B. M. Jelenković
Institute of Physics, University of Belgrade, Pregrevica 118, RS-11080 Belgrade, Serbia
(Received 1 August 2011; published 25 October 2011)

We studied experimentally and theoretically the evolution of open atomic systems in the constant intensity laser field. The study is performed by analyzing the line shapes of Hanle electromagnetically induced transparency (EIT) obtained in different segments of a laser beam cross section of constant intensity, i.e., a Π-shaped laser beam. Such Hanle EIT resonances were measured using a small movable aperture placed just in front of the photodetector, i.e., after the entire laser beam had passed through the vacuum Rb cell. The laser was locked to the open transition $F_g = 2 \rightarrow F_e = 1$ at the D_1 line of ^{87}Rb with laser intensities between 0.5 and 4 mW/cm^2. This study shows that the profile of the laser beam determines the processes governing the development of atomic states during the interaction. The resonances obtained near the beam center are narrower than those obtained near the beam edge, but the significant changes of the linewidths occur only near the beam edge, i.e., right after the atom enters the beam. The Hanle EIT resonances obtained near the beam center exhibit two pronounced minima next to the central maximum. The theoretical model reveals that the occurrence of these transmission minima is a joint effect of the preparation of atoms into the dark state and the optical pumping into the uncoupled ground level $F_g = 1$. The appearance of the transmission minima, although similar to that observed in the wings of a Gaussian beam [A. J. Krmpot *et al.*, Opt. Express **17**, 22491 (2009)], is of an entirely different nature for the Π-shaped laser beam.

DOI: 10.1103/PhysRevA.84.043844 PACS number(s): 42.50.Gy, 42.50.Nn, 42.62.Fi, 42.65.−k

I. INTRODUCTION

Coherent effects in Doppler-broadened alkali-metal-atom vapors have been intensively investigated because of numerous applications of phenomena based on such coherent effects. Coherent population trapping (CPT) [1,2], electromagnetically induced transparency (EIT) [3], and electromagnetically induced absorption (EIA) [4] have been observed and examined in either pump-probe or Hanle configurations [5,6]. All these phenomena strongly depend on the intensity of the applied laser field and consequently also on the radial profile of the intensity of the laser beam. Most often, in experiments, the radial laser beam profile is Gaussian, while theoretical models assume that the intensity of the laser field is constant across the diameter of the laser beam. The latter will be referred to throughout this paper as the Π laser beam. For the interaction of the Gaussian or Π laser beam with alkali-metal-atom vapor, the different effects such as Ramsey and Dicke narrowing, transit time, and Doppler broadening are examined either in vacuum [7,8] or in buffer gas cells [9–12] The differences in EIT line shapes for Gaussian and Π laser beams were presented in [13–15] by considering only the entire laser beam contribution without focusing on the details of laser-atom interaction within the laser beam. However, different parts of the laser beam cross section, after passing through the alkali-metal vapor cell, carry different information about the atomic state and yield different EIT resonances [16].

In this paper we study time and space evolution of atomic states as the Rb atoms traverse the Π-shaped laser beam, i.e., electric field of nearly constant intensity. Such studies were performed by measuring EIT line shapes from different circular segments of the laser beam cross section, much smaller than the laser beam diameter, and after the entire beam had first passed through the Rb cell. We used a Hanle configuration with the laser locked to the $F_g = 2 \rightarrow F_e = 1$ hyperfine transition of the D_1 line in the ^{87}Rb isotope in the vacuum vapor cell. Similar examinations of the EIT resonances in different segments, but for the Gaussian laser beam cross section, were performed in an effusive regime in the Rb vacuum cell [16] and in a diffusive regime in the dense $^4He^+$ vapor [17]. Due to interaction with a laser electric field having different distributions in the Gaussian and Π-shaped beams, the atomic state develops differently in the presence of a small external magnetic field. Narrowing of the Hanle EIT in the wings of the Gaussian laser beam is observed and explained by the interference of the laser light and coherently prepared atoms coming from the central part of the beam [16]. Such Ramsey-type narrowing of dark-state resonances was studied also in different geometries in Refs. [18,19]. The narrowing is accompanied by the appearance of Ramsey-like transmission minima in Hanle EIT line shapes detected in the Gaussian beam wings. Therefore, it is expected that examination of EIT line shapes obtained in different segments of Π laser beam cross section should reveal some details about the transient evolution of interacting atoms. It can also help in understanding differences in linewidths and amplitudes of EIT resonances obtained using two laser beam profiles and reported in Refs. [13–15]. To our knowledge, partial Hanle EIT from different segments of the Π laser beam was not thoroughly investigated. The significance of using the Π profile is in the elimination of the effects due to transverse variation of the laser intensity, providing conditions for more direct insight into the laser-atom interaction. Experimental results of the spatial dependence of EIT line shapes along the laser beam profile are compared with the theoretical calculations. The theoretical model is based on time-dependent optical Bloch equations (OBEs) predicting the evolution of the

*krmpot@ipb.ac.rs

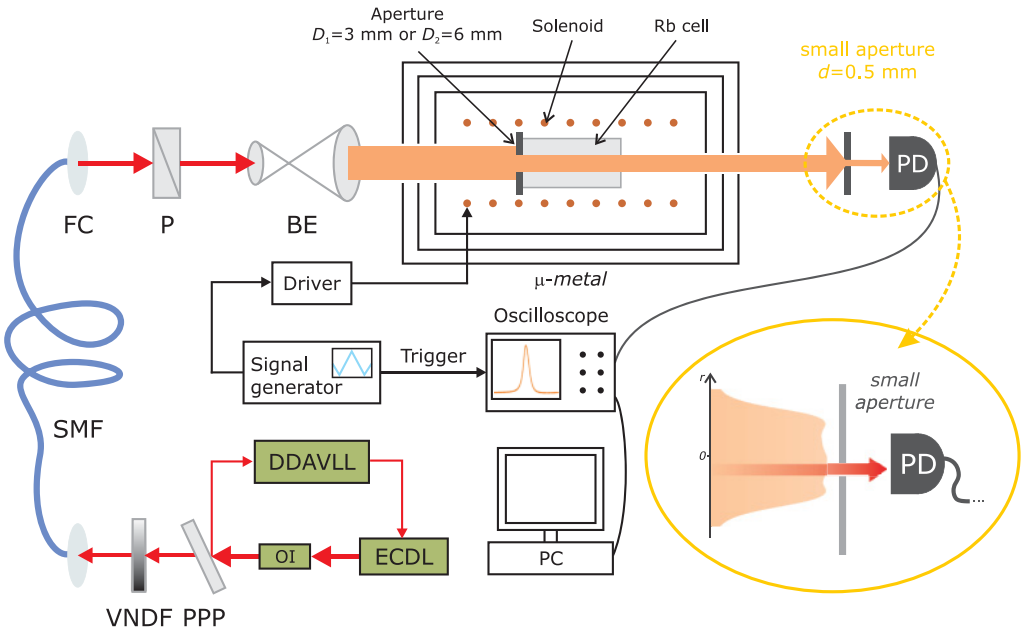

FIG. 1. (Color online) (a) Experimental setup: ECDL - external cavity diode laser; OI - optical isolator; DDAVLL - Doppler-free dichroic atomic vapor laser lock; VNDF - variable neutral density filter; PPP - plan parallel plate; SMF - single-mode fiber; FC - fiber collimator; P - polarizer; BE - beam expander; PD - photodiode. The aperture moved on the translation stage allows only a selected part of the laser beam to reach the detector, while the rest of the laser beam is blocked.

Zeeman sublevel populations and coherences in the laser field of profiled intensity. It unveils the influence of the optical pumping into the uncoupled ground-state hyperfine level on the obtained Hanle EIT line shapes.

II. EXPERIMENT

The experimental setup is shown in Fig. 1. The external cavity diode laser is frequency locked to the $F_g = 2 \rightarrow F_e = 1$ transition of the D_1 line in ^{87}Rb, where F_g and F_e represent the angular momenta of the ground- and excited-state hyperfine levels, respectively. Laser locking is performed in an auxiliary vacuum Rb cell using the Doppler-free dichroic atomic vapor laser lock (DDAVLL) method [20,21]. The variable neutral density filter is used for laser power adjustments. Single-mode fiber was used to provide the Gaussian laser beam. After passing through the Glan-Thompson polarizer, the laser beam becomes linearly polarized. The Π-shaped laser beam profile was obtained after expanding the Gaussian laser beam from the single-mode fiber to 20 mm in diameter and then extracting its central part using the circular aperture placed on the entrance window of the cell. After experimenting with different diameters of the expanded Gaussian laser beam, sizes of apertures, and thicknesses of the foil used for the apertures, we obtained the Π-shaped laser beam whose radial intensity profiles have the least pronounced diffraction effects as shown in Fig. 2. The beam profiles measured by the beam profiler are 3 cm [Figs. 2(a) and 2(c)] and 30 cm [Figs. 2 (b) and 2(d)] away from the 3- or 6-mm aperture on 0.1-mm-thick foil. The first profile is at a distance equal to the distance between the aperture and the midsection of the Rb cell. This profile is referred to as Π-shaped throughout the paper. We used the beam profile at 30 cm from the aperture to show relatively small changes in the profile with distance and to justify use of the Π-shaped profile in the theoretical model. A well-collimated Π-shaped laser beam then passes through the 6-cm-long vacuum Rb cell containing a natural abundance of rubidium isotopes. The cell is placed in the solenoid used for scanning the axial magnetic field between -100 and $+100$ μT. The cell and the solenoid are placed inside the triple-layered μ-metal cylinders to eliminate Earth's and stray magnetic fields. In order to measure Hanle EIT from only small parts of the laser beam cross section, a movable aperture of 0.5 mm in diameter is placed in front of the photodiode with a large detection surface (area, 80 mm^2). "Small aperture" will henceforth refer to an 0.5-mm aperture in order to differ from the 3- or 6-mm aperture used for laser beam shaping, placed in front of the Rb cell. By moving this small aperture with the precise translation stage we allow only light from a small segment of the transmitted laser beam to reach the photodiode, after the entire beam passes through the Rb cell. The signal obtained from this photodiode while scanning the external magnetic field is recorded by the digital oscilloscope and transferred to the computer.

III. THEORETICAL MODEL

Hanle EIT resonances were calculated for the D_1 line transition $F_g = 2 \rightarrow F_e = 1$ of ^{87}Rb coupled to a linearly polarized laser in a Rb vacuum cell. The energy level diagram given in Fig. 3 shows hyperfine levels either coupled to the laser light or populated due to spontaneous emission. The quantization z axis is chosen to be parallel to the external magnetic field. The complete magnetic sublevel structure is considered in calculations. The model is based on

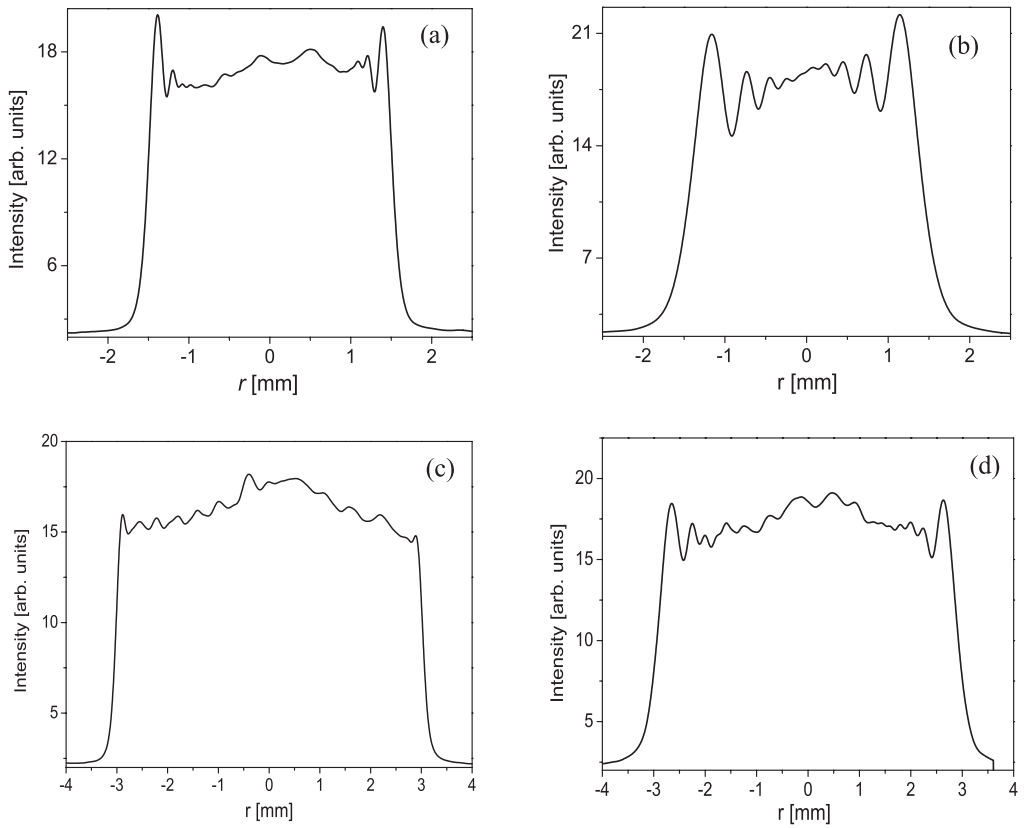

FIG. 2. Two Π-shaped beam profiles recorded by a beam profiler placed at different distances from the circular aperture: at 3 cm (a) and 30 cm (b) for the 3-mm profile, and at 3 cm (c) and 30 cm (d) for the 6-mm profile.

time-dependent optical Bloch equations for the density matrix of a moving atom,

$$\dot{\rho} = -\frac{i}{\hbar}\left[H_{\text{atom}}(B) + H_{\text{int}}(t), \rho\right] + \dot{\rho}_{\text{SE}}, \tag{1}$$

where

$$H_{\text{atom}}(B) = \sum_j \hbar\omega_j(B)|g_j\rangle\langle g_j| + \sum_k \hbar\omega_k(B)|e_k\rangle\langle e_k| \tag{2}$$

is the atomic Hamiltonian corresponding to ground (excited) states $|g_j\rangle \equiv |F_g, m_g = j\rangle$ ($|e_k\rangle \equiv |F_e, m_e = k\rangle$) with

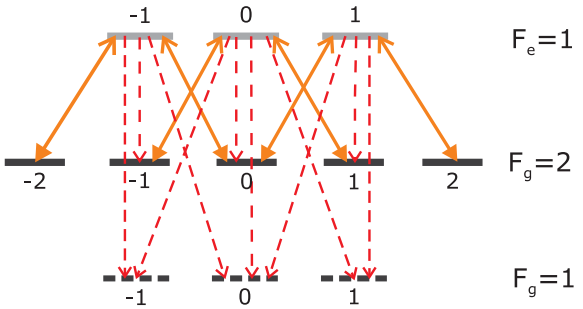

FIG. 3. (Color online) Zeeman sublevel scheme in ^{87}Rb at the D_1 line. The solid lines denote coupling with σ^+ and σ^- components of linearly polarized laser light. Dashed lines represent spontaneous emission.

Zeeman-shifted energies $\hbar\omega_j(B)$ [$\hbar\omega_k(B)$] in the external magnetic field B. Laser-atom interaction is given by

$$H_{\text{int}}(t) = -\sum_{j,k} \mathbf{E}(t)\cdot\mathbf{d}_{jk}(|g_j\rangle\langle e_k| + |e_k\rangle\langle g_j|), \tag{3}$$

where $\mathbf{E}(t)$ is the time-dependent laser electrical field and $\mathbf{d}_{jk}$ is the atomic electric dipole moment for the transition between states $|g_j\rangle$ and $|e_k\rangle$. Spontaneous emission is included through the Lindblad-form term

$$\dot{\rho}_{\text{SE}} = \frac{\Gamma}{2}\sum_m 2A_m\rho A_m^\dagger - A_m^\dagger A_m\rho - \rho A_m^\dagger A_m, \tag{4}$$

where $\Gamma = 2\pi \times 5.746$ MHz is the D_1 line decay rate of the excited state and A_m are operators corresponding to dipole transitions from the excited- to ground-state manifold, leading to

$$\langle e_i|\dot{\rho}_{\text{SE}}|e_j\rangle = -\Gamma\rho_{e_ie_j}, \quad \langle e_i|\dot{\rho}_{\text{SE}}|e_j\rangle = -\frac{\Gamma}{2}\rho_{e_ig_j},$$

$$\langle g_i|\dot{\rho}_{\text{SE}}|g_j\rangle = (-1)^{i+j}(2F_e+1)\Gamma_{F_e\to F_g}\sum_{q=-1}^{1}\begin{pmatrix} F_e & 1 & F_g \\ j+q & -q & -j\end{pmatrix} \times \begin{pmatrix} F_e & 1 & F_g \\ i+q & -q & -i\end{pmatrix}\rho_{e_{i+q}e_{j+q}}. \tag{5}$$

$\Gamma_{F_e \to F_g}$ is the decay rate from F_e to one F_g ground hyperfine level given by

$$\Gamma_{F_e \to F_g} = (2J_e + 1)(2F_g + 1)\begin{Bmatrix} J_g & J_e & 1 \\ F_e & F_g & I_g \end{Bmatrix}^2 \Gamma, \qquad (6)$$

where J and I represent the electron and nuclear angular momentum quantum numbers. Equations for density matrix elements related to the $F_g = 1$ ground level are excluded since that level is not coupled by the laser. For additional details please refer to [15]. It is assumed that after colliding with cell walls, atoms reset into an internal state with equally populated ground magnetic sublevels. Between collisions with cell walls, rubidium atoms interact only with the axially oriented homogeneous magnetic field and spatially dependent laser electric field. Collisions among Rb atoms are negligible due to very low Rb vapor pressure at room temperature, so an atom moves through the laser beam with constant velocity $\mathbf{v} = \mathbf{v}_\parallel + \mathbf{v}_\perp$, where $\mathbf{v}_\parallel$ and $\mathbf{v}_\perp$ are velocity components parallel and perpendicular to laser propagation direction, respectively. The former affects the longitudinal direction of the atomic trajectory and Doppler shift of the laser frequency seen by a moving atom, while the latter determines the transverse direction of the trajectory and the interaction time. The dependence of the laser intensity on the radial distance r for a Π-shaped profile was modeled using the following equation:

$$I(r) = \bar{I}a\{1 + \mathrm{erf}\,[p(r_0 - r)]\}^2, \qquad (7)$$

where r_0 is the beam radius, $\bar{I}$ is the beam intensity (total laser power divided by ${r_0}^2\pi$), a is the normalization constant, and p is a positive parameter affecting the steepness of the profile near $r = r_0$. In our calculations we neglect longitudinal changes of the beam profile compared to transverse ones so that only the transverse direction of the trajectory matters. Therefore, we drop the explicit dependence on z of all physical quantities. From the reference frame of the moving atom, the electric field varies and the rate of variation depends only on $\mathbf{v}_\perp$. Assume that the transverse projection of the atomic trajectory is given by

$$\mathbf{r}_\perp(t) = \mathbf{r}_{0\perp} + \mathbf{v}_\perp t, \qquad (8)$$

where $\mathbf{r}_{0\perp}$ is the perpendicular component of the atom position vector at $t = 0$. The temporal variation of the laser intensity seen by the atom is given by

$$I(t) \equiv I(\mathbf{r}_\perp(t)) = I(\mathbf{r}_{0\perp} + \mathbf{v}_\perp t), \qquad (9)$$

representing the spatial laser intensity variation along the trajectory of the atom in the laboratory frame. Additionally, due to the cylindrical symmetry of the beam profile, spatial dependence becomes purely radial dependence. The observed resonances in EIT experiments are a probabilistic average of the contributions of many individual, mutually noninteracting atoms. Rb atoms traverse the laser beam at different trajectories with different velocities. Maxwell-Boltzmann velocity distribution, diversity of atomic trajectories, and custom cylindrically symmetric radial profile of the laser electric field are treated similarly as in [15]. The trajectories having different distances from the laser beam center are chosen so that the beam cross section is uniformly covered (Fig. 4). The chosen trajectories correspond to different angles ϕ defined as shown in the Fig. 4. For a representative set of atomic velocities the atomic density matrix $\rho(B;\mathbf{v};\mathbf{r}_\perp)$ along a given trajectory is calculated assuming constant magnetic field B during the atomic transit through the laser beam. To obtain the atomic ensemble density matrix $\rho(B;r)$ across the beam cross section for a set of radial distances r, the calculated density matrices are first averaged over the Maxwell-Boltzmann velocity distribution. Furthermore, by integrating the density matrix over all trajectories containing points with radial distances in the interval $(r,r + \Delta r)$ the contribution $\rho(B;r)$ of a certain segment of the laser beam cross section is obtained. In our case $\Delta r = 0.5$ mm corresponds to the diameter of the collecting aperture. Owing to the cylindrical symmetries of the laser beam profile and the atomic velocity distribution, the velocity-averaged density matrix will also be cylindrically symmetric. Thus, the angular integral appearing in the averaging over velocity $\mathbf{v}(\phi) = (\phi, v_\perp, v_\parallel)$ can be replaced by an angular integral over space

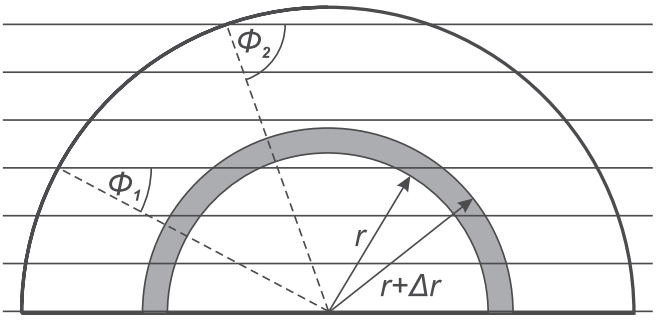

FIG. 4. Schematic of atomic trajectories chosen to cover the entire laser beam cross section (horizontal straight lines). Each trajectory defines certain angle ϕ, e.g., ϕ_1 and ϕ_2. The contribution of each segment, like the gray ring segment, is obtained by integrating the density matrix over all trajectories containing points with radial distances in the interval $(r,r + \Delta r)$.

$$\rho(B;r) = \int_0^{2\pi} \frac{d\phi}{2\pi} \int_0^\infty dv_\perp W_\perp(v_\perp) \int_{-\infty}^\infty dv_\parallel W_\parallel(v_\parallel) \times \rho(B;0,v_\perp,v_\parallel;r\cos\phi, r\sin\phi), \qquad (10)$$

with the Maxwell-Boltzmann velocity distribution given by

$$W_\perp(v_\perp) = \frac{2v_\perp}{u^2} e^{-(v_\perp/u)^2}, \quad W_\parallel(v_\parallel) = \frac{1}{u\sqrt{\pi}} e^{-(v_\parallel/u)^2}, \qquad (11)$$

where $u = (2k_B T/m_{\mathrm{Rb}})^{1/2}$ is the most probable velocity of Rb atoms at temperature T.

The effects of the laser propagation along the cell and induced atomic polarization of the Rb vapor are included using the following approximations. We first compute the Rb vapor ensemble density matrix $\rho(B;r)$ and polarization $\mathbf{P}$ assuming the constant value of the electric field $\mathbf{E}$ along the z direction of laser propagation within the cell. The polarization of Rb vapor is obtained from the ensemble density matrix

$$\mathbf{P}(B;r) = n(T)\,\mathrm{Tr}[\rho(B;r)\,e\hat{\mathbf{r}}], \qquad (12)$$

where the ^{87}Rb concentration at temperature T is given by [22]

$$\log_{10} n(T) = \log_{10}\left(0.2783 \times \frac{133.322}{k_B T}\right) - 94.0483 - 0.0377169\,T - 1961.26/T + 18.4902\log_{10}(T). \quad (13)$$

Due to trace operation including dipole operator $e\hat{\mathbf{r}}$, the polarization $\mathbf{P}$ depends only on the optical coherences between the ground and the excited Zeeman sublevels. Using the computed Rb polarization, we calculate the change of the electric field due to propagation of the laser through the Rb vapor. Assuming that the change of electric field along the length L of the Rb cell is small enough, the exact relation

$$\frac{\partial \mathbf{E}(B;r,z)}{\partial z} = \frac{i\omega_0}{2\epsilon_0 c}\mathbf{P}(B;r,z) \quad (14)$$

in the first approximation takes the form

$$\mathbf{E}(B;r,z=L) = \mathbf{E}(B;r,z=0) + \frac{i\omega_0}{2\epsilon_0 c}\mathbf{P}(B;r)L, \quad (15)$$

where ϵ_0 is the vacuum dielectric constant and ω_0 is the laser frequency. The transmitted electric field of Eq. (15) is used in the calculations of Hanle EIT resonances. The cell temperature was set to 25 °C as in experiments.

IV. RESULTS AND DISCUSSION

Experimental and theoretical Hanle EIT resonances obtained at different positions of the small aperture along the beam diameter are presented in Figs. 5(a) and 5(b), respectively. Hereafter $r = 0$ mm refers to the center of the laser beam cross section. The beam diameter is 3 mm and overall intensity is 4 mW/cm^2. Results in Fig. 5 show significant differences in shapes, widths, and amplitudes of resonances obtained at different positions within the cross section of the Π profiled laser beam. The Hanle EIT resonances originating from the central parts of the Π beam cross section exhibit two transmission minima next to the central maximum of the EIT resonance. Further, resonances in the center of the laser beam cross section are narrower than those originating from the outer parts of the beam. These results are reversed to the results obtained from different segments of a Gaussian laser beam cross section. In the latter case two minima appear, and the resonances are narrower, when the small aperture is placed at the wings of the Gaussian beam cross section [16].

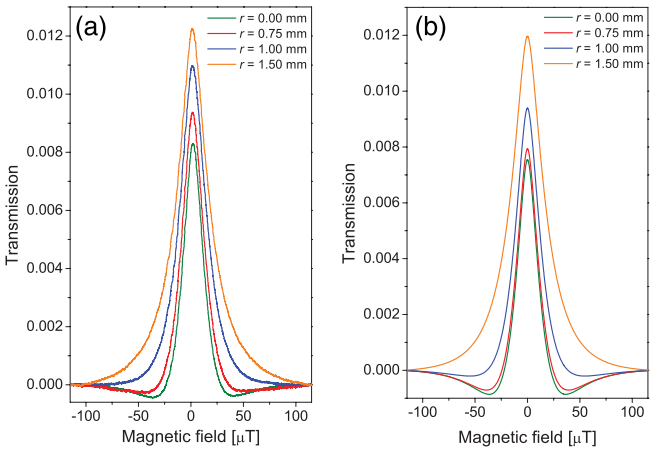

FIG. 5. (Color online) Experimental (a) and theoretical (b) Hanle EIT resonances obtained from the small segments of the Π beam cross section. Green, red, blue, and orange curves are for $r = 0$ mm, 0.75 mm, 1.0 mm and 1.5 mm, from bottom to top, respectively, where r is the radial distance of the small aperture from the beam center. The beam diameter is 3 mm and the total intensity is 4 mW/cm^2. The theoretical results were normalized to the experimental results at $r = 0$ mm.

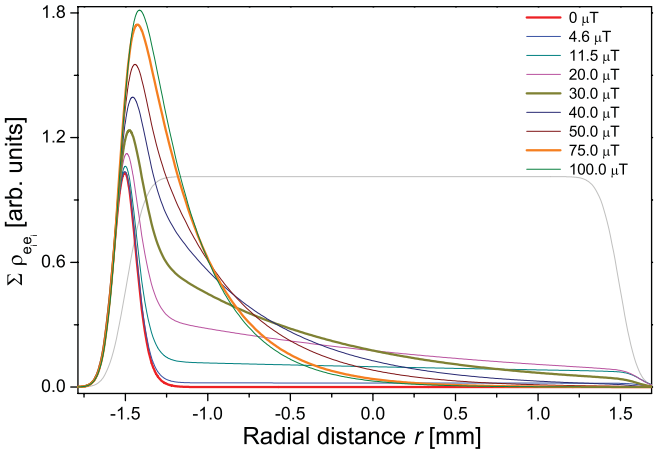

FIG. 6. (Color online) Calculated total population $\sum \rho_{e_i e_i}$ of all Zeeman sublevels of the $F_e = 1$ excited level at different magnetic fields as a function of position along the 3-mm beam diameter of the Π-shaped laser beam. The curves corresponding to the magnetic fields 0–100 μT from the legend appear from bottom to top, respectively, at $r = -1.25$ mm. The beam intensity is 4 mW/cm^2. The atomic velocity is 180 m/s at temperature 300 K. The thin gray line represents the cross section of the laser beam with an arbitrary intensity unit. The atom enters the beam from the left.

Neglecting small intensity variations of the Π-shaped laser beam (see Fig. 2) atoms interact with a constant electric field of the laser in the presence of constant external magnetic field during the passage through the laser beam. The evolution of the atomic state under these conditions is different than in the case of the Gaussian beam. In Fig. 6 we present a calculated variation of the total population of the excited state $F_e = 1$ as a function of distance from the entrance in the laser beam (leftmost), considering atoms with the most probable radial velocity of 180 m/s at room temperature (300 K). When an atom enters the laser beam at zero magnetic field ($B = 0$), it starts to absorb photons and the population of the excited state, i.e., the sum of the populations of all excited-state Zeeman sublevels, increases (red thick line in Fig. 6). Shortly after entering the laser beam, atoms are prepared into the dark state and do not absorb photons afterward yielding maximal transmission. At small magnetic fields the preparation of atoms into the dark state is less efficient and there is certain probability for photon absorption during the entire interaction of the atom and the laser light. Thus, the excited-state population decreases less rapidly than for $B = 0$ as atoms move through the laser beam and transmission decreases. As Fig. 6 shows, the atomic total excited-state population, for atoms near the laser beam center, is largest for a magnetic field at about 30 μT (dark yellow thick

line) when transmission reaches minimum. At larger magnetic fields (e.g., 75 μT, orange thick line), pumping into the uncoupled $F_g = 1$ hyperfine level becomes considerable and transmission noticeably increases. The observed behavior of the excited-state populations and resulting laser transmission are due to the fact that the rates of pumping into the dark state and into the uncoupled level depend oppositely on the external magnetic field. Therefore, the appearance of two transmission minima at about 30 μT is a joint effect of preparation of atoms into the dark state and optical pumping into the uncoupled ground hyperfine level.

Behavior of the excited-level population at different magnetic fields explains the origin of the two symmetrically placed, with respect to the central transmission peak, transmission minima present in the Hanle EIT resonances recorded near the center of the laser beam. For a given laser intensity, atoms have to spend a certain time in the laser beam before these minima emerge in the Hanle EIT curves. It turns out that if the laser beam has a 3-mm diameter, for most atoms this shape of the EIT would only be observed in the laser beam center. If one considers a laser beam with a diameter lager than 3 mm, under the same experimental conditions (the same cell temperature, i.e., the most probable velocity, and the same laser intensity), it is expected that optical pumping would significantly affect EIT line shapes at the same distances of ~1.5 mm from the edge of the beam. Consequently, with the larger beam diameter, transmission minima should occur in the wider area around the beam center. The curves in Fig. 7 present experimental and theoretical Hanle EIT resonances obtained at different positions of the small aperture along the 6-mm diameter Π-shaped laser beam. Overall intensity is similar as before, 4 mW/cm^2. Now, transmission minima are present in Hanle EIT resonances obtained not only in the center of the laser beam, but also up to a certain distance away from the center. Moreover, the resonances obtained up to that distance

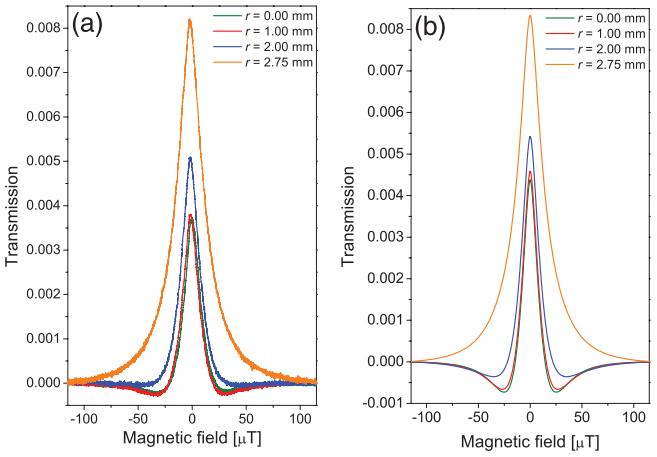

FIG. 7. (Color online) Experimental (a) and theoretical (b) Hanle EIT resonances obtained from the small segments of the Π laser beam cross section at four distances from the beam center: 0, 1.0, 2.0, and 2.75 mm (from bottom to top, respectively). The beam diameter is 6 mm and the total laser intensity is 4 mW/cm^2. The theoretical results were normalized to the experimental results at $r = 0$ mm. Note that the curves for $r = 0$ and $r = 1.0$ mm almost overlap.

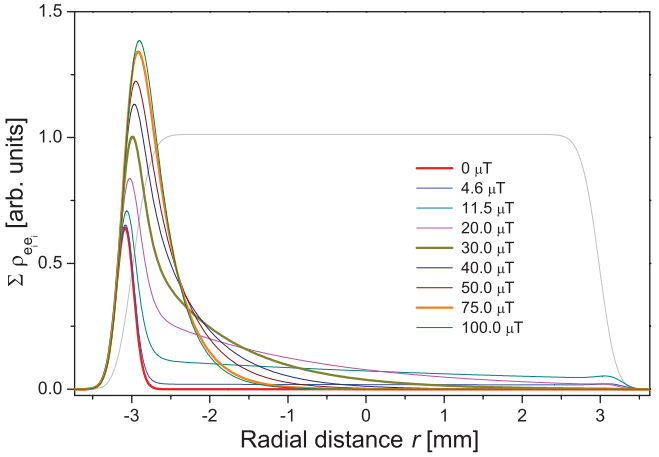

FIG. 8. (Color online) Calculated total population $\sum \rho_{e_i e_i}$ of all Zeeman sublevels of the $F_e = 1$ excited level at different magnetic fields as a function of position along the 6-mm beam diameter of Π-shaped laser beam. The curves corresponding to the magnetic fields 0–100 μT from the legend appear from bottom to top, respectively, at $r = -2.75$ mm. The beam intensity is 4 mW/cm^2 intensity. The atomic velocity is the most probable velocity at room temperature (180 m/s). The thin gray line represents the laser beam cross section profile.

are almost the same, as in the case of overlapping resonances for $r = 0$ and $r = 1$ mm in Fig. 7.

The explanation for the appearance of transmission minima in Hanle EIT line shapes in the case of a 6-mm-diameter laser beam could be made tracing the behavior of the total excited-state populations given in Fig. 8 and applying the same logic as in Fig. 6, i.e., for the 3-mm beam diameter. It is apparent from Figs. 6 and 8 that under the same experimental conditions, the distance from the beam edge where the total excited-state population at $B = 75$ μT (orange thick line) falls down to zero is the same in both cases, approximately 1.5 mm. For the 3-mm beam diameter this point coincides with the location of the beam center, while for the 6-mm-diameter beam this location is, of course, away from the beam center. Therefore for the 6-mm-diameter beam, transmission minima in Hanle EIT resonances at around $B = 30$ μT will occur as long as EIT resonances are taken from the central region of 3 mm in diameter.

To further clarify the influence of optical pumping on Hanle EIT line shapes we performed calculations by artificially closing the transition $F_g = 2 \rightarrow F_e = 1$, i.e., eliminating the optical pumping. Calculated Hanle EIT resonances, for the laser intensity of 4 mW/cm^2, are shown in Fig. 9. Obtained Hanle EIT line shapes are broader than for the open system because there is no population-loss-induced narrowing [23,24]. The absence of population loss also yields the same line shapes regardless of the distance from the beam center. There is no transmission minima in line shapes obtained at the central regions of the beam cross section. In this case, a slight increase of transmission at very large magnetic fields (~200 μT) is due to the broad single-photon Hanle background on which the EIT resonances are superimposed. Next, we investigate the influence of the overall laser intensity on line shapes of the EIT obtained in different segments of the Π-shaped laser beam. The curves in Figs. 10(a) and 10(b) are experimental

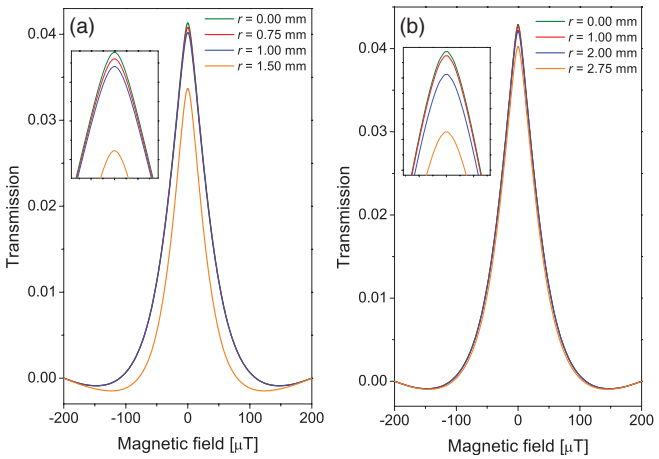

FIG. 9. (Color online) Calculated Hanle EIT resonances obtained from the small segments of the Π laser beam cross section of (a) 3 mm and (b) 6 mm diameter. It is assumed that the transition $F_g = 2 \rightarrow F_e = 1$ is closed. The resonances almost completely overlap and can be barely distinguished only near $B = 0$ (see insets). The curves corresponding to decreasing radial distances from the legends appear from bottom to top, respectively. The laser intensity is 4 mW/cm^2. Note a different scale for the magnetic field than in Figs. 5 and 7 and a broadening of resonances in the case of the closed transition.

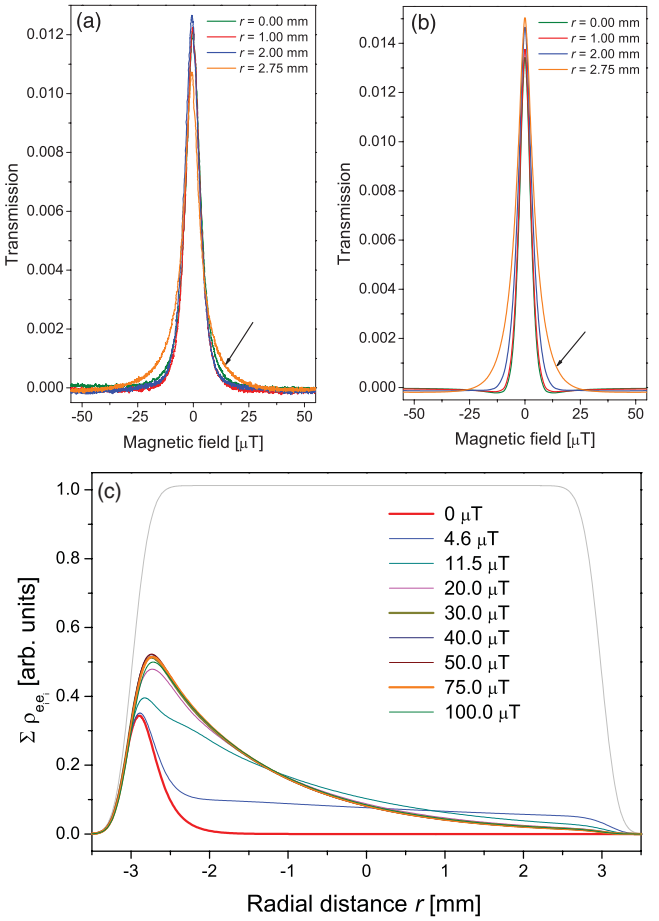

FIG. 10. (Color online) Experimental (a) and theoretical (b) Hanle EIT resonances obtained from the small segments of the Π laser beam cross section at four distances r from the beam center. The resonances are nearly identical except for the resonance obtained close to rim of the beam (pointed to with the arrow). The beam diameter is 6 mm and the total intensity is 0.5 mW/cm^2. Note that the magnetic field range is smaller than in Figs. 5 and 7. (c) Calculated total population of all Zeeman sublevels of the $F_e = 1$ excited level at different magnetic fields as a function of position along the 6-mm beam diameter of Π-shaped laser beam. The curves corresponding to the magnetic fields 0–100 μT from the legend appear from bottom to top, respectively, at $r = -2.5$ mm. The curves for $B \gtrsim 20$ μT are almost identical. The atomic velocity is the most probable velocity at room temperature (180 m/s). The thin gray line represents the laser beam cross section profile.

and theoretical Hanle EIT resonances obtained for the laser intensity 0.5 mW/cm^2 at different positions of the small aperture along the beam diameter of 6 mm. At lower laser intensity, transmission minima are missing (experiment) or barely visible (theory) in the Hanle EIT profiles, because of the weak optical pumping. Since there are diffraction effects between the planes of the two apertures (see Fig. 1) the radial position of the collecting aperture does not map exactly the corresponding position in the atomic cell. This introduces some averaging that may explain why the structures are smoother in the experiments with respect to the calculations. In Fig. 10(c) we show the total excited-state populations for an atom traversing the beam with velocity 180 m/s as a function of the radial distance from the beam center at different magnetic fields. Even at a very high magnetic field (75 μT), the population is not zero as it was at high laser intensities (see Fig. 8) because optical pumping to the $F_g = 1$ level is not as efficient. In this case the transmission of the vapor will not increase at high magnetic fields and consequently there are no transmission minima at Hanle EIT resonance profiles at any position along the beam diameter.

As discussed above, EIT line shapes obtained in different parts of the Π-shaped laser beam cross section are determined by evolution of the dark states and (particularly around the beam center) by the optical pumping. On the other hand, the change of atomic coherence in the magnetic field is found to play a significant role in the line shapes obtained in parts of the Gaussian laser beam cross section [16]. Results in Figs. 11(a) and 11(b) confirm different mechanisms responsible for EIT line shapes for two radial profiles of the laser beam. Here we compare the calculated phase of the coherence, induced between the $m_F = -1$ and $m_F = 1$ Zeeman sublevels of $F_g = 2$ hyperfine level for atoms passing through the Gaussian and the Π laser beam. The magnetic field during transit time of an atom is assumed constant. The results are shown for those magnetic fields at which transmission minima appear in Hanle EIT resonances, i.e., 10 μT (30 μT) for the Gaussian (Π) laser beam. Both beams have the same average intensity. Since the laser electric field tends to keep the phase of the coherence constant while the magnetic field tends to change the phase, when both magnetic and electric field are present, the phase of atomic coherence depends on the magnitudes of these two fields. The atom is coherently prepared and the phase is kept fixed by the laser field in the central parts of the Gaussian beam. In the wings of the Gaussian beam the phase value of the same atomic coherence depends on the local laser intensity.

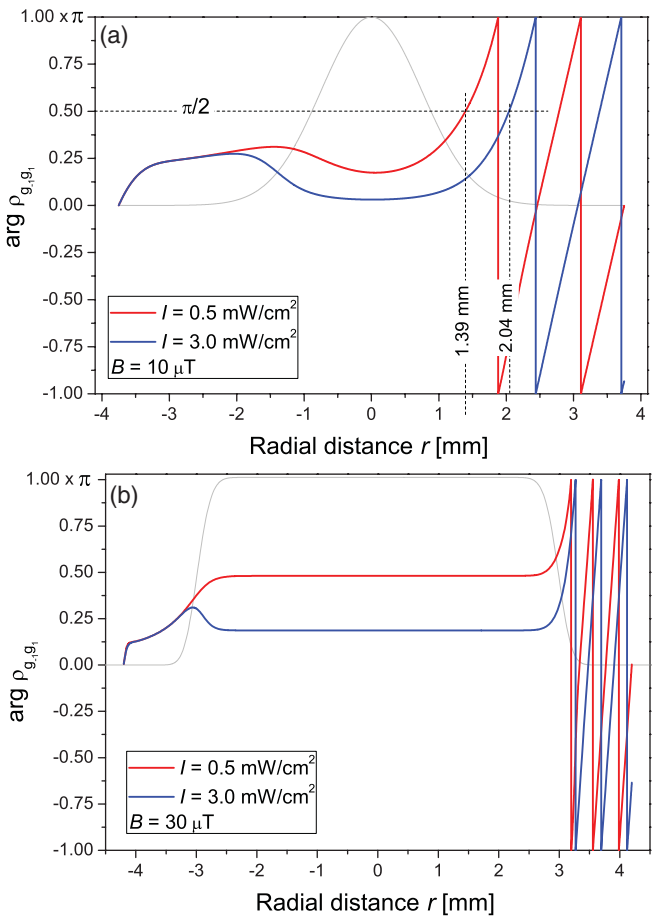

FIG. 11. (Color online) (a) Change of the argument of atomic coherence ρ_{g_{-1},g_1} during atom passage through the 3-mm-wide Gaussian laser beam at constant magnetic field. The dashed lines denote the positions along the beam radius where the Hanle EIT resonances exhibit very pronounced transmission minima. The transmission minima at the Hanle EIT resonances appear in the wings of the Gaussian beam cross section when arg ρ_{g_{-1},g_1}, i.e., the atomic phase is equal to $\pi/2$ [16]. (b) Change of the argument of atomic coherence during atom passage through the 6-mm-wide Π laser beam at constant magnetic field. It is obvious that the phase is constant during atom passage through the Π laser beam, regardless of the laser intensity. The magnetic field values of 10 μT and 30 μT for the Gaussian and Π laser beams, respectively, are chosen because the transmission minima in the Hanle EIT resonances appear exactly at those values in corresponding laser beam profiles. The beam profile is presented by the gray line.

When the atomic phase reaches $\pi/2$, i.e., the atomic state becomes bright, two transmission minima appear in Hanle EIT resonances obtained in the wings of the Gaussian laser beam [16]. In a constant and strong field of the Π-shaped laser beam, the phase of the coherence is constant across the beam and therefore it is not the change of the phase that affects the observed Hanle EIT line shapes.

Physical processes leading to line narrowing or broadening of coherent resonances were extensively studied under different experimental conditions, laser beam geometries, and cell dimensions [7–12,16,25–28]. Figures 12(a) and 12(b) show experimental and theoretical results for the dependence

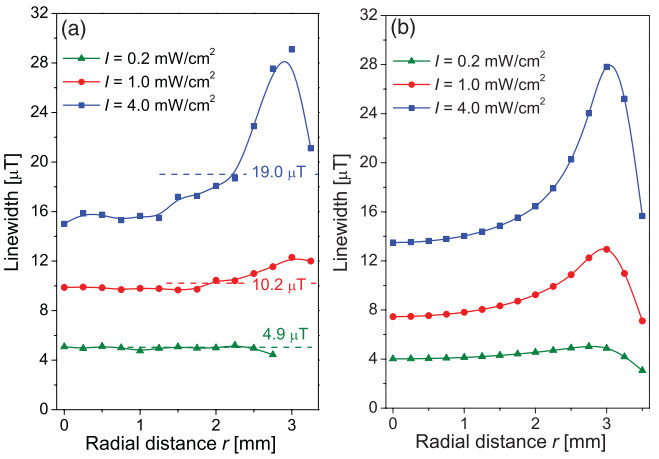

FIG. 12. (Color online) (a) Experimental and (b) theoretical Hanle EIT linewidths at different positions of small aperture along the 6-mm-diameter Π-shaped laser beam. I is the laser intensity. The dashed lines in (a) denote the Hanle EIT linewidths when the whole laser beam is detected.

of linewidths of the Hanle EIT resonances on the radial position r of the small aperture along the 6-mm diameter of the Π-shaped laser beam. The dashed lines in Fig. 12(a) denote the Hanle EIT linewidths when the whole laser beam is detected. Results are given for three different laser intensities. It is obvious that there is Hanle EIT line narrowing from the edge toward the beam center. This is population-loss-induced transit time narrowing [23,24]. As seen in Fig. 12, it is more pronounced at higher laser intensities, when most significant Hanle EIT narrowing apparently occurs in the region close to the beam edges, i.e., very soon after the atom enters the beam.

Important information about atomic evolution during interaction with the constant intensity laser field can be obtained by comparing the linewidths of the Hanle EIT resonances for central and outer regions of the Π laser beam cross section and for the whole beam, at different laser intensities. Figure 13 shows Hanle EIT linewidths versus laser intensity for (a) 3 - and (b) 6-mm beam diameters. For the 3-mm diameter Π laser beam, the linewidths are presented for resonances in the center ($r = 0$), for the resonances obtained at the outer region of the beam ($r = 1.5$ mm) and when the whole beam is detected. The resonances measured in the center of the laser beam cross section are noticeably narrower. For the 6-mm-diameter Π laser beam, besides resonances at the center ($r = 0$), at the edge ($r = 3$ mm), and for the whole beam, the linewidths of resonances obtained at $r = 1.5$ mm are also presented. The results for $r = 1.5$ mm support the discussion related to Fig. 8. It is shown that the most rapid changes of atomic state, for atoms with the most probable radial velocity, occur shortly after the atom enters the laser beam, i.e., after passing a distance of about 1.5 mm from the beam edge. Figure 13(b) shows that the resonances recorded close to the laser beam edge ($r = 3$ mm) are significantly wider than those from the inner parts of the beam ($r = 1.5$ mm and $r = 0$). In addition, an expanded laser beam (6-mm diameter) causes narrower resonances in the center of the beam cross section and also

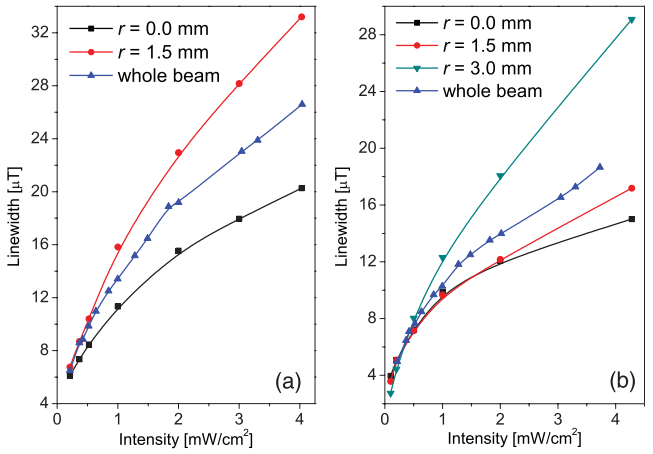

FIG. 13. (Color online) Dependence of Hanle EIT resonance linewidths from the laser intensity for the central regions of the Π laser beam cross section, the circumference region, and the whole beam. Results are shown for two laser beam diameters (a) 3 and (b) 6 mm. The results for the $r = 1.5$ mm in case of the 6-mm-diameter beam are presented for better comparison because this radius coincides with the edge of the 3-mm-diameter beam.

for the whole beam, comparing to the smaller beam diameter (3 mm).

The results from Fig. 13 show that as the diameter of the Π-shaped laser beam increases, the contribution of the Hanle EIT from the rim of the beam cross section to the whole beam resonance linewidth decreases. In other words, when increasing the laser beam diameter the whole beam resonance becomes more similar to those from the inner region of the laser beam cross section.

V. SUMMARY

We have studied the evolution of atomic states in constant magnetic and laser fields using Π-shaped laser beam resonant to the open $F_g = 2 \rightarrow F_e = 1$ transition in ^{87}Rb. This laser radial profile allows such studies to be unaffected by intensity variations of the laser electric field. Information about the transient evolution of the atomic state during the interaction with the laser beam was obtained by detailed analysis of features in line shapes of the Hanle EIT resonances from small segments of the laser beam cross section. Experimentally and theoretically these resonances were obtained by sampling the transmitted laser light at various positions of the small aperture along the radius of a well-collimated laser beam, after the entire beam had passed through the Rb cell. We have shown that considerable absorption occurs immediately after atoms enter the laser beam. At low magnetic fields this leads to the efficient preparation into a dark state and consequent evolution with low photon absorption throughout the inner region of the beam cross section. At higher magnetic fields, the initial absorption is followed by optical pumping into an uncoupled ground hyperfine level which dominates the behavior of the atomic state throughout the laser beam cross section. The appearance of transmission minima, as sidebands to the EIT resonance, in the inner regions of the laser beam is due to strong dependence of optical pumping on the magnetic field. Transmission minima were also observed for Hanle EIT resonances obtained using the Gaussian laser beam, but such EIT line shapes were only observed in the wings of the beam [16]. Their presence was attributed to the interference of the laser light in the beam wings and coherently prepared atoms coming from the central part of the beam. Thus, essentially different physical mechanisms, *optical pumping (incoherent)* in Π laser beams and *Ramsey-like effect (coherent)* in Gaussian laser beams, yield seemingly similar results, i.e., the appearance of the transmission minima in Hanle EIT line shapes. In addition, the observed narrowing of Hanle EIT resonances toward the center of the Π-shaped laser beam cross section is induced by population loss during the atomic transit through the laser beam. It is apparent that for the proper modeling of experiments and identification and understanding of dominant processes affecting the dark-state evolution within the laser beam, it is essential to take into account a real beam profile.

ACKNOWLEDGMENTS

This work was supported by the Ministry of Education and Science of the Republic of Serbia, under Grants No. III45016 and No. OI171038.

[1] E. Arimondo, Prog. Opt. **35**, 257 (1996).
[2] G. Alzetta, A. Gozzini, L. Moi, and G. Orriolis, Nuovo Cimento **36**, 5 (1976).
[3] S. E. Harris, J. E. Field, and A. Imamoglu, Phys. Rev. Lett. **64**, 1107 (1990).
[4] A. M. Akulshin, S. Barreiro, and A. Lezama, Phys. Rev. A **57**, 2996 (1998).
[5] G. Moruzzi and F. Strumia, *The Hanle Effect and Level Crossing Spectroscopy* (Plenum, New Yrk, 1991).
[6] C. Andreeva, S. Cartaleva, Y. Dancheva, V. Biancalana, A. Burchianti, C. Marinelli, E. Mariotti, L. Moi, and K. Nasyrov, Phys. Rev. A **66**, 012502 (2002).
[7] E. Pfleghaar, J. Wurster, S. I. Kanorsky, and A. Weis, Opt. Commun. **99**, 303 (1993).
[8] S. Knappe, M. Stähler, C. Affolderbach, A. V. Taichenachev, V. I. Yudin, and R. Wynands, Appl. Phys. B **76**, 57 (2003).
[9] Y. Xiao, I. Novikova, D. F. Phillips, and R. L. Walsworth, Phys. Rev. Lett. **96**, 043601 (2006).
[10] Y. Xiao, I. Novikova, D. F. Phillips, and R. L. Walsworth, Opt. Express **16**, 14128 (2008).
[11] O. Firstenberg, M. Shuker, R. Pugatch, D. R. Fredkin, N. Davidson, and A. Ron, Phys. Rev. A **77**, 043830 (2008).
[12] S. Mitra, M. M. Hossain, B. Ray, P. N. Ghosh, S. Cartaleva, and D. Slavov, Opt. Commun. **283**, 1500 (2010).
[13] F. Levi, A. Godone, J. Vanier, S. Micalizio, and G. Modugno, Eur. Phys. J. D **12**, 53 (2000).

[14] A. V. Taichenachev, A. M. Tumaikin, V. I. Yudin, M. Stahler, R. Wynands, J. Kitching, and L. Hollberg, Phys. Rev. A **69**, 024501 (2004).
[15] M. Radonjić, D. Arsenović, Z. Grujić, and B. M. Jelenković, Phys. Rev. A **79**, 023805 (2009).
[16] A. J. Krmpot, S. M. Ćuk, S. N. Nikolić, M. Radonjić, D. G. Slavov, and B. M. Jelenković, Opt. Express **17**, 22491 (2009).
[17] H. Gilles, B. Cheron, O. Emile, F. Bretenaker, and A. Le Floch, Phys. Rev. Lett. **86**, 1175 (2001).
[18] Z. D. Grujić, M. Mijailović, D. Arsenović, A. Kovacević, M. Nikolić, and B. M. Jelenković, Phys. Rev. A **78**, 063816 (2008).
[19] B. Schuh, S. I. Kanorsky, A. Weis, and T. W. Hänsch, Opt. Commun. **100**, 451 (1993).
[20] G. Wasik, W. Gawlik, J. Zachorowski, and W. Zawadzki, Appl. Phys. B **75**, 613 (2002).
[21] T. Petelski, M. Fattori, G. Lamporesi, J. Stuhler, and G. M. Tino, Eur. Phys. J. D **22**, 279 (2003).
[22] A. N. Nesmeyanov, *Vapor Pressure of the Chemical Elements*, edited by R. Gray (Elsevier, Amsterdam, 1963).
[23] F. Renzoni, W. Maichen, L. Windholz, and E. Arimondo, Phys. Rev. A **55**, 3710 (1997).
[24] F. Renzoni and E. Arimondo, Phys. Rev. A **58**, 4717 (1998).
[25] M. Auzinsh, R. Ferber, F. Gahbauer, A. Jarmola, L. Kalvans, A. Papoyan, and D. Sarkisyan, Phys. Rev. A **81**, 033408 (2010).
[26] D. Sarkisyan, D. Bloch, A. Papoyan, and M. Ducloy, Opt. Commun. **200**, 201 (2001).
[27] C. Andreeva, A. Atvars, M. Auzinsh, K. Blush, S. Cartaleva, L. Petrov, and D. Slavov, Phys. Rev. A **76**, 063804 (2007).
[28] E. Alipieva, S. Gateva, E. Taskova, and S. Cartaleva, Opt. Lett. **28**, 1817 (2003).